Lasers in Surgery and Medicine 42:680–688 (2010)

Experimental Validation of the Effects of Microvasculature Pigment Packaging on In Vivo Diffuse Reflectance Spectroscopy

Narasimhan Rajaram, PhD, Ashwini Gopal, MS, Xiaojing Zhang, PhD, and James W. Tunnell, PhD*
Department of Biomedical Engineering, The University of Texas at Austin, Austin, Texas

Background: Diffuse reflectance spectroscopy (DRS) uses the steady-state diffuse reflectance measured from the tissue surface to determine absorption and scattering properties of sampled tissue. Many inverse models used to determine absorber properties have assumed a homogeneous distribution of blood. However, blood in tissue is confined to blood vessels that occupy a small fraction of the overall volume. This simplified assumption can lead to large errors when measuring optical properties. The objective of this study was to examine the effect of confining absorbers to small volumes, such as the microvasculature, on in vivo DRS.

Study Design: We fabricated multi-layer microfluidic devices to mimic blood vessels with a size similar to skin microvasculature. We studied the effect of varying channel size (diameter = 22 and 44 μm) and absorber concentration (10–80% food color dye in water) on diffuse reflectance measurements. We also examined the in vivo reflectance from normal skin and non-melanoma skin cancer on 14 patients.

Results: Our results demonstrate that both absorption coefficient and vessel diameter affect the diffuse reflectance spectra. An empirically calculated packaging correction factor based on our experiments shows good agreement with previous theoretical derivations of the same factor. In vivo measurements on normal skin and basal cell carcinoma show that incorporating a correction factor greatly improves the fit of the inverse model to the spectra. In addition, there were statistically significant differences in measured mean vessel diameter and blood volume fraction between normal skin and basal cell carcinoma.

Conclusion: We have demonstrated experimentally the effect of pigment packaging in blood vessels over a physiologically relevant range of blood vessel size and absorption. The correction factors implemented to account for the packaging effect could potentially be used as diagnostic parameters for diagnosing skin cancers. Lasers Surg. Med. 42:680–688, 2010. © 2010 Wiley-Liss, Inc.

Key words: diffuse reflectance; pigment packaging; microfluidics

INTRODUCTION

Over the past few years, several studies have reported the use of diffuse reflectance spectroscopy (DRS) techniques for non-invasively monitoring the optical properties and hence physiology of tissue for various applications. A model-based analysis of diffuse reflectance can provide volume-averaged quantitative estimates of the scattering and absorption of sampled tissue [1–5]. In spectrally resolved diffuse reflectance measurements, the scattering and absorption properties of tissue are constrained parameters over the wavelength range of interest. In the visible range, the absorption coefficient [$\mu_a(\lambda)$] of tissue is assumed to be a linear combination of absorbers specific to the tissue type sampled such as hemoglobin in blood, beta-carotene, and melanin. Most experimental measurements of the absorption coefficients of oxygenated and deoxygenated hemoglobin, in particular, are based on a homogeneous solution of hemoglobin. On the contrary, blood in tissue is confined to a very small fraction of the overall volume, namely blood vessels.

Duysens first demonstrated, with chlorophyll, that the absorption spectrum of any suspension (confined distribution) of absorbing particles must appear flattened as compared to a homogeneous distribution of the same [6]. Hemoglobin, for instance, has two primary bands of absorption: the Soret (peak = 420 nm) and *Q*-bands (peaks = 542 and 577 nm), with the former being the dominant absorption band. A confined distribution of very high concentrations of hemoglobin can significantly reduce the optical path length at 420 nm. This results in a flattening of the Soret absorption bands relative to the *Q*-bands. Such an effect is referred to as pigment or vessel packaging. This effect manifests itself in and affects spectrally resolved diffuse reflectance measurements. Hence, an analytical model that uses the absorption spectrum of a homogeneous solution of hemoglobin to fit such flattened spectra can significantly over-estimate

Contract grant sponsor: ASLMS Student Research Grant; Contract grant sponsor: Wallace H. Coulter Foundation; Contract grant sponsor: National Institutes of Health; Contract grant number: R01 CA132032.
*Correspondence to: James W. Tunnell, PhD, Department of Biomedical Engineering, The University of Texas at Austin, University Station C0800, Austin, TX 78712.
E-mail: jtunnell@mail.utexas.edu
Accepted 13 April 2010
Published online in Wiley Online Library (wileyonlinelibrary.com).
DOI 10.1002/lsm.20933

the absorption coefficient measured from diffuse reflectance spectra. Finlay and Foster [7] reported a spectral flattening, by as much as 65%, of the absorption spectrum of hemoglobin confined to erythrocytes as compared to a homogeneous solution of the same. They also showed a good improvement in the accuracy of fitting diffuse reflectance spectra by accounting for this phenomenon. Several research studies have employed Monte–Carlo simulations [8,9] to derive an expression for the packaging effect. Liu et al. [10] used a heterogeneous resin-tube model with large vessel diameters (~1–3 mm) to demonstrate the influence of blood vessel distribution on hemoglobin oxygenation measurements using time resolved spectroscopy. van Veen et al. [11] demonstrated the use of a correction factor that has subsequently been used in several in vivo research studies to determine the blood volume fraction and the dimensions of the volume to which blood is confined, typically the mean blood vessel diameter. The objective of this study was to examine the effect of pigment packaging over a physiological range of absorption and vessel sizes relevant to epithelial microvasculature.

Epithelial microvasculature has a particular significance in the use of DRS for the early diagnosis of cancer as most cancers form near the tissue surface in epithelial tissues. We are currently conducting a pilot clinical study to determine the diagnostic accuracy of a non-invasive spectral diagnosis system for classifying non-melanoma skin cancers (NMSC), which form in the skin's epithelium (or epidermis). Our system combines two optical modalities—diffuse reflectance and laser-induced fluorescence spectroscopy and employs a model-based quantitative analysis to determine the physiological parameters of tissue [12]. Because our diagnostic algorithm is based on physiological parameters measured using the model, it is important to ensure that the model accounts for the effect of pigment packaging and avoids overestimating the absorption properties of tissue.

The pigment packaging studies mentioned previously were based on either Monte–Carlo simulations or experiments using blood vessel-like structures that were not in a range of values (~1–3 mm) relevant for epithelial microvasculature. However, there are no known experimental studies that have studied the effect of pigment packaging for blood vessel sizes typically found in the upper layers of skin (~10–100 μm) or other epithelial tissues. In fact, a few studies have used the packaging correction factor to measure the mean blood vessel diameter from in vivo [13] and ex vivo [14] measurements. The values for mean vessel diameter reported in their studies are in the range of 10–30 μm. Our motivation for this project was to demonstrate, for the first time to our knowledge, the effect of pigment packaging with controlled experiments on tissue-simulating phantoms containing blood vessel-like structures in a range of values relevant to epithelial microvasculature. We used multi-layer microfluidic devices with channels that mimicked the blood vessels found in the epithelium. Based on experiments on these microfluidic devices, we calculated an empirical correction factor to account for the effect of packaging. Our results show that the empirically calculated correction factor based on microfluidic devices has a very similar behavior to the correction factor previously presented by van Veen [11] and used by others [13–15], over a physiologically relevant range of tissue absorption and vessel sizes. We incorporated this correction factor in our inverse model to measure optical properties of NMSC and normal skin. Our results show that accounting for the effect of packaging significantly improves the goodness of fit of our inverse model to measured diffuse reflectance spectra. In vivo measurements demonstrate that the measured mean vessel diameter and blood volume fraction are significantly different between normal skin and NMSC and can potentially be used as diagnostic parameters for classifying NMSC.

THEORY

For a homogenous distribution of absorber, the absorption coefficient can be computed as a simple product of the extinction coefficient and concentration of the absorber. Assuming hemoglobin as the absorber, this equation can be expressed as,

$$\mu_a(\lambda) = [\mathrm{Hb}] \times [\alpha\varepsilon_{\mathrm{HbO_2}}(\lambda) + (1-\alpha)\varepsilon_{\mathrm{Hb}}(\lambda)] \quad [\mathrm{mm}^{-1}] \quad (1)$$

where [Hb] is the total hemoglobin concentration sampled by the light, α is the oxygen saturation representing the ratio of oxygenated to total hemoglobin concentration and $\varepsilon_{\mathrm{HbO_2}}(\lambda)$ and $\varepsilon_{\mathrm{Hb}}(\lambda)$ are the extinction coefficients of oxygenated and deoxygenated hemoglobin, respectively. To incorporate the effect of pigment packaging, we use van Veen's [11] equation to describe the correction factor,

$$C_{\mathrm{pack}} = \left[\frac{1-\exp(-2\mu_{a,bl}(\lambda)r_{\mathrm{vess}})}{2\mu_{a,bl}(\lambda)r_{\mathrm{vess}}}\right] \quad (2)$$

where $\mu_{a,bl}(\lambda)$ is the absorption coefficient of whole blood and r_{vess} is assumed to be the mean vessel radius in the tissue volume sampled. We assume the hemoglobin concentration in whole blood to be 150 mg/ml [16] in order to calculate the value of mean vessel radius using Equation (2). The absorption coefficient of whole blood can be calculated using Equation (1) as:

$$\mu_{a,bl}(\lambda) = 150 \times [\alpha\varepsilon_{\mathrm{HbO_2}}(\lambda) + (1-\alpha)\varepsilon_{\mathrm{Hb}}(\lambda)] \quad [\mathrm{mm}^{-1}] \quad (3)$$

The packaging corrected absorption coefficient of a tissue-like medium can now be written as:

$$\mu_a^{\mathrm{corr}}(\lambda) = C_{\mathrm{pack}}\nu\mu_{a,bl}(\lambda) \quad [\mathrm{mm}^{-1}] \quad (4)$$

where ν denotes the blood volume fraction assuming a hemoglobin concentration of 150 mg/ml. The blood volume fraction is a measure of the effective or volume-averaged hemoglobin concentration that is sampled by the light, assuming the whole blood hemoglobin concentration in the blood vessels is 150 mg/ml.

Equation (2) indicates that the correction factor C_{pack} is a function of both vascular diameter and the absorption coefficient inside a confined volume. The dependence of C_{pack} on $2\mu_{a,bl}(\lambda)\, r_{\mathrm{vess}}$ is illustrated in Figure 1. The plot

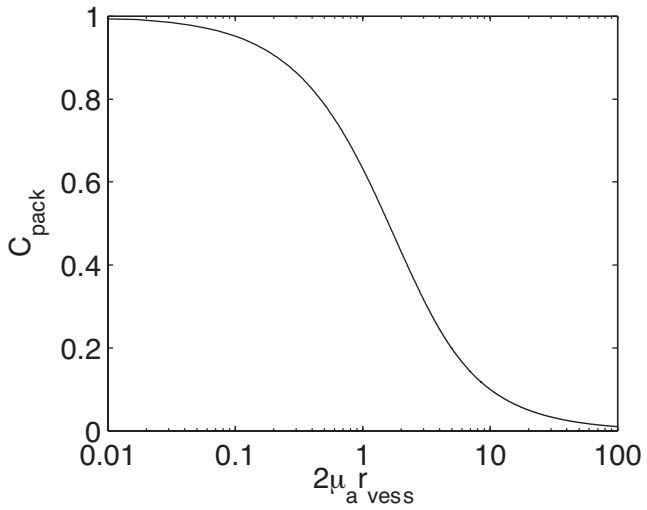

Fig. 1. Packaging correction factor as a function of the optical depth parameter ($2\mu_a r_{\mathrm{vess}}$).

shows that for small vascular diameters or lower concentrations, the effect of packaging is almost negligible with a C_{pack} value approximately equal to 1. However, as the blood vessel size or absorber concentration inside the vessel increases, the value of C_{pack} decreases, indicating the need for a larger correction. As part of our experiments on microfluidic devices, we will use Equation (1) to fit the diffuse reflectance spectra and determine an empirical value for the packaging correction factor.

MATERIALS AND METHODS

DRS System

The experimental setup consisted of the following components: (1) a white-light tungsten halogen lamp to illuminate the sample (LS-1; Ocean Optics, Dunedin, FL), (2) a 16-bit spectrometer (USB4000; Ocean Optics, Dunedin, FL) to record the diffusely reflected light, and (3) a fiber optic probe (FiberTech Optica, Ontario, Canada) with a 350 μm source-detector separation. The fibers were arranged in a 6-around-1 configuration with the central fiber illuminating the sample and the six surrounding fibers collecting the diffusely reflected light. We used an integration time of 15 ms to acquire measurements. Reflectance measurements made on each day were calibrated according to procedures already described [12].

Microfluidic Devices

Figure 2 shows a schematic of a microfluidic device consisting of three thin polydimethylsiloxane (PDMS) layers with uniformly embedded titanium dioxide (TiO_2) particles (the PDMS:TiO_2 layer). We use TiO_2 (size <5 μm; Sigma–Aldrich, St. Louis, MO) to simulate scattering in the device. We mixed 1.8 mg of TiO_2 per gram of PDMS to create a reduced scattering coefficient of approximately $1\,\mathrm{mm}^{-1}$ at 630 nm. We fabricated two sets of devices with channel height and width (aspect ratio 1:1) 22 and 44 μm. The thickness of the PDMS:TiO_2 microfluidic layer and the number of channels in each layer was varied according to the channel size to maintain the overall volume fraction of the channels. For both 22 and 44 μm devices, the thickness of the top layer was 200 μm. The thickness of the two subsequent layers in the 22 μm device was 200 μm, while the thickness was 400 μm for the 44 μm device. A clear layer of PDMS (devoid of TiO_2) was bonded to the top of the microfluidic layers (Fig. 2a). The purpose of this layer was to provide device structural support as well as the common access ports for the tubing into the microfluidic channels. This layer is only present on top of the inlet and outlet ports and does not cover the microfluidic channels. The well-aligned multi-layer microfluidic device was then bonded to a 5-mm thick homogeneous PDMS:TiO_2 slab to simulate a semi-infinite medium.

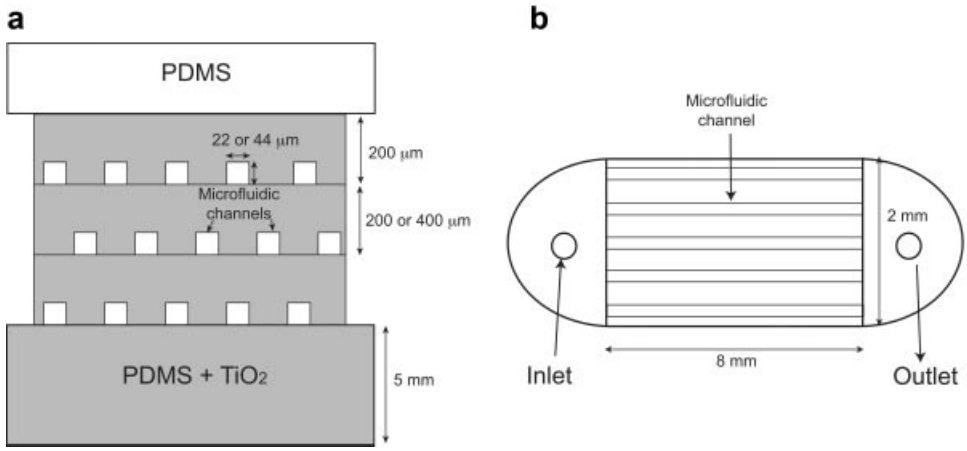

Fig. 2. **a**: Schematic representation of a multi-layer microfluidic device. The second and third layers are 200 or 400 μm depending on the channel height (22 or 44 μm, respectively). **b**: Top view.

The PDMS (Sylgard 184; Dow Corning Corp, Midland, MI) channels were fabricated based on the rapid prototyping technique [17]. SU8 photoresist (Microchem Corp., Newton, MA) was patterned photolithographically on a silicon wafer using specifications provided by Microchem Corp. (http://www.microchem.com/resources/download.asp?file=SU-8-microfluidicIII). Depending on the channel height specification for our device, SU8-2020 and SU8-2050 (~20 and ~40 μm thickness) was used. Channels with feature size 22 and 44 μm were created as SU8 master molds. The PDMS:TiO_2 mixture was then spin coated over the SU8 master mold, cured at 70°C for ~30 min, and peeled off the mold to form the microchannel structures. The thickness of the PDMS:TiO_2 layer containing the microfluidic channels can be tuned by varying the spin speed. The PDMS:TiO_2 layers were bonded using oxygen plasma technique. Holes were punched for inlets and outlets for silicone tubing of the microfluidic devices.

DRS Measurements

We measured the diffusely reflected light from the two sets of fabricated microfluidic devices using different concentrations of absorber. We used red food color dye (McCormick, Sparks, MD) as the absorber. We used concentrations of 10%, 30%, 50%, 70%, and 80% (v/v) absorbing dye dissolved in de-ionized water. The dye concentrations used and their corresponding volume-averaged concentrations and absorption coefficients are shown in Table 1. Note that column 1 refers to the dye concentrations that were pumped through the channels. Column 2 represents the volume-averaged concentration in the device and column 3 represents the volume-averaged absorption coefficient of the dye over the entire spectral range (450–700 nm). The volume-averaged dye concentrations spanned an absorption (μ_a) range of 0–1.99 mm^{-1}. In comparison, a typical value for volume-averaged blood absorption in tissue is approximately 1–2 mm^{-1} in the Soret absorption band (410–430 nm). We also measured the reflectance spectrum from a homogeneous phantom containing the same volume-averaged dye concentrations as the microfluidic devices and 1-μm diameter polystyrene beads (Polysciences, Warrington, PA) to simulate scattering.

TABLE 1. Absorbing Dye Concentrations (v/v%) That Were Injected Through the Channels and Corresponding Volume-Averaged Dye Concentrations for the Microfluidic Devices

Dye concentration (%)	Volume-averaged dye concentration (%)	μ_a [mm^{-1}]
10	0.08	0–0.25
30	0.24	0–0.75
50	0.4	0–1.24
70	0.56	0–1.74
80	0.64	0–1.99

The absorption coefficients shown here are also volume-averaged values for the microfluidic devices.

We used an injection pump to pump the dye through the channels. We used a low injection rate of ~1 μl/min to avoid damaging the channels. We placed the fiber optic probe directly over the channels and in contact with the top layer of the device. Diffusely reflected light is recorded in the wavelength range of 450–700 nm. Diffuse reflectance was calculated as a ratio of background-corrected diffuse white light intensity recorded from a phantom to the background-corrected white light intensity measured from a 20% reflectance standard (Labsphere, North Sutton, NH). Each measurement was repeated three times by flushing the device and re-injecting the absorbing dye.

In Vivo DRS on Skin

We are currently conducting a clinical feasibility study on non-melanoma and melanoma skin cancers at the University of Texas Medical Branch, Austin (UTMB) and the Mohs surgery clinic at the M.D. Anderson Cancer Center, Houston (MDACC). The Institutional Review Boards (IRB) at both institutions approved the study protocol. The clinical system used in the study has already been described previously [12] and acquires in vivo diffuse reflectance and intrinsic fluorescence measurements from skin. We have collected spectral measurements from 40 patients who were diagnosed with one of the following types of NMSC based on pathology: (1) basal cell carcinoma (BCC), (2) squamous cell carcinoma (SCC), and (3) actinic keratosis (AK). In this study, we discuss our clinical results from the BCC group of lesions. We have measured 23 normal spectra and 39 lesion spectra from 18 different BCC lesions.

DRS Inverse Model

We used a lookup table (LUT)-based inverse model to fit the acquired DRS spectra and measure the scattering and absorption properties of the sample. The development and validation of the LUT model has been described in detail in the literature [5]. Briefly, the LUT is a database of experimental reflectance measurements made on calibration standards of known optical properties and is specific to our probe geometry. By spectrally constraining the scattering and absorption coefficients, we can fit the LUT to our diffuse reflectance spectra and recover the scattering and absorption properties of sampled tissue. The LUT has a demonstrated error of less than 10% in determining the scattering and absorption properties of tissue-simulating phantoms. We constrained the reduced scattering coefficient to the form,

$$\mu_s'(\lambda) = \mu_s'(\lambda_0) \times \left[\frac{\lambda}{\lambda_0}\right]^{-B} \quad [\mathrm{mm}^{-1}] \tag{5}$$

where $\lambda_0 = 630$ nm. Researchers have shown that a power law dependence on wavelength is an appropriate approximation of scattering in bulk tissue [18]. $\mu_s'(\lambda_0)$ and B are indicators of scattering magnitude and scatterer size, respectively. We use Equation (5) to describe scattering from the microfluidic phantoms as well as in vivo skin. We calculated the absorption coefficient using Equation (1) as,

$$\mu_a(\lambda) = [\text{dye}] \times \varepsilon_{\text{dye}}(\lambda) \quad [\text{mm}^{-1}] \tag{6}$$

where ε_{dye} denotes the extinction of the absorber (red dye) used and [dye] represents the dye concentration.

Based on the constraining equations described above, we implemented a Levenberg–Marquadt nonlinear optimization fitting routine to fit the model to the measured diffuse reflectance spectra. Based on the initial values of the fit parameters—$\mu_s'(\lambda_0)$, B, and [dye]—the model calculated the absorption and scattering coefficients as a function of wavelength using Equations (5) and (6). The fitting routine minimized the residual between the measured and calculated reflectance spectra and determined the fit with the lowest residual. The fit values corresponding to the lowest residual were returned as extracted optical properties of the phantom or sampled skin. We constrained the fit parameters to vary within a physiologically relevant range.

RESULTS

DRS Measurements

Figure 3a shows the absorption spectrum of a 100% (v/v) solution of absorber measured using a UV–Vis spectrophotometer (DU-720; Beckman Coulter, Brea, CA). The red food color dye has an absorption peak at 525 nm. The measured diffuse reflectance spectra from the homogeneous phantom, 22 and 44 μm devices for varying dye concentrations are shown in Figure 3b–d, respectively. The trough in the reflectance spectrum is due to absorption by the dye, while the general shape of the reflectance curve is derived either from the scattering behavior of TiO_2 or polystyrene beads, depending on the phantom. The magnitudes of the reflectance spectra from the microfluidic devices for different concentrations are approximately equal for wavelengths greater than 600 nm. This is expected because the dye absorption does not extend beyond this wavelength and only scattering from the phantom contributes to the signal. This is also true for the homogeneous phantom; however, the slope of the phantom appears different due to the choice of scatterer.

Figure 4a presents a comparison of the homogeneous phantom and microfluidic devices with 10% (v/v) absorber concentration. The homogeneous phantom contained the volume-averaged dye concentration corresponding to 10% in the microfluidic devices. We normalized the reflectance spectra to the reflectance at 630 nm (R_{630}) to compare spectra from the microfluidic devices. For the same volume-averaged dye concentration, the reflectance from the microfluidic phantoms appears flattened when compared to the homogeneous phantom and the degree of flattening increases as we progress to the 44 μm device. The

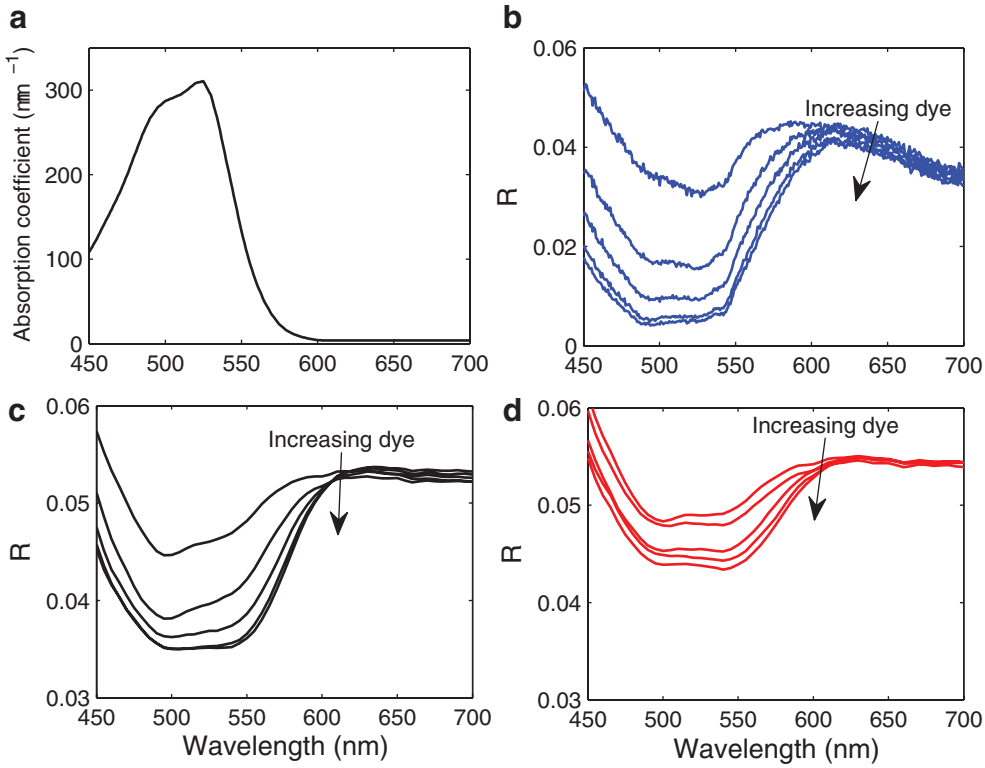

Fig. 3. **a**: Absorption spectrum of 100% (v/v) red color dye used in the microfluidic experiments. Spectrally resolved diffuse reflectance for varying dye concentrations within (**b**) a homogeneous phantom and injected through microfluidic devices with (**c**) 22 μm channels and (**d**) 44 μm channels.

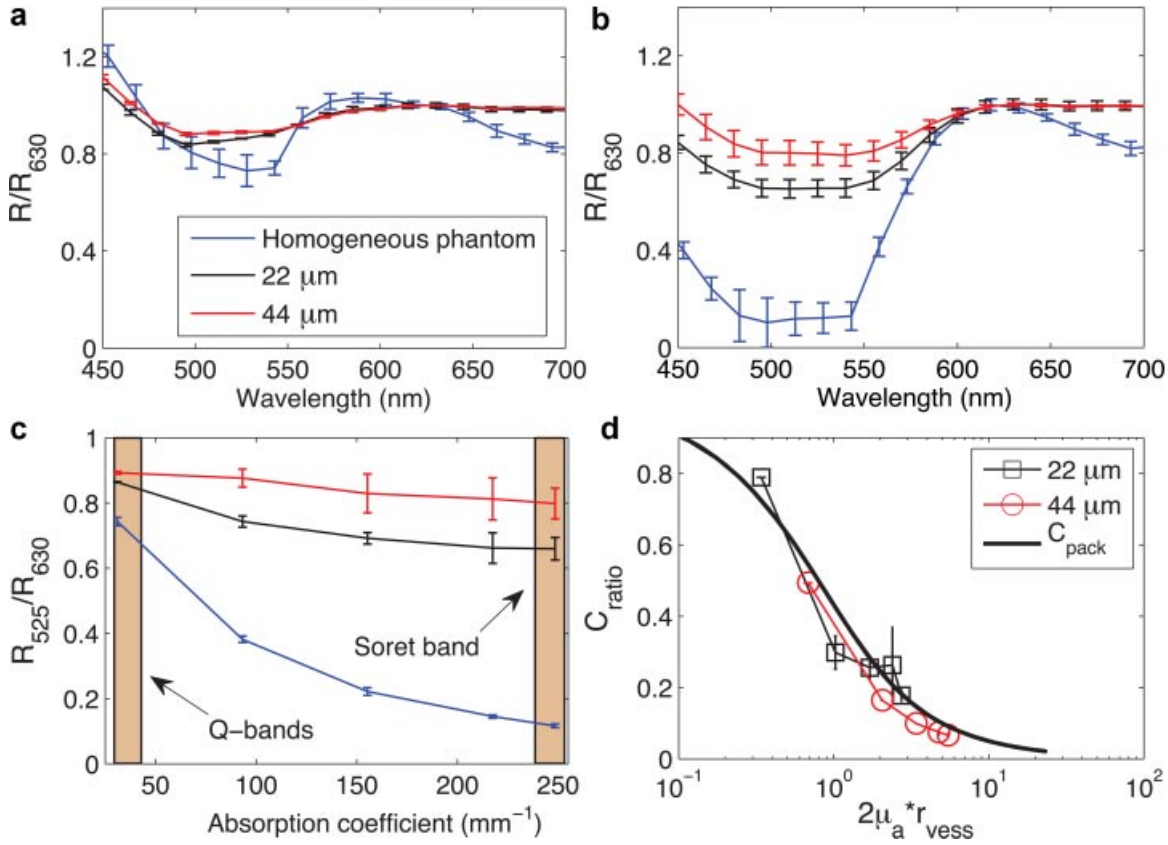

Fig. 4. Comparison of diffuse reflectance for the same volume-averaged dye concentration injected through 22 and 44 μm devices and within a homogeneous phantom—(**a**) 10% dye and (**b**) 80% dye. Spectra are normalized to reflectance at 630 nm (R/R_{630}). **c**: Diffuse reflectance at the peak absorption wavelength (R_{525}) for varying dye concentrations normalized to R_{630} (R_{525}/R_{630}). **d**: C_{ratio} calculated for the 22 and 44 μm devices, overlaid on C_{pack} as presented in Figure 1. Error bars represent 1 SD.

effect of packaging is clearly seen in the reflectance spectra at the highest absorber concentration (80%). Figure 4b shows the same trend in flattening of the reflectance spectra, albeit to a much greater degree than Figure 4a. These plots demonstrate that the effect of packaging depends both on absorber concentration as well as the volume of confinement. In addition, the dye concentrations in Figure 4a,b are in the same range of absorption coefficients of blood in the *Q*-bands and Soret band, respectively. Therefore, these plots demonstrate the effect of packaging with respect to physiological conditions.

Figure 4c shows the normalized diffuse reflectance at the peak absorption wavelength of the absorbing dye (525 nm) normalized to R_{630}, for both devices and the homogeneous phantom. The reflectance from the homogeneous dye phantom drops to almost 90% of its initial value as we increase the dye concentration from 10% to 80%. In the absence of packaging, this is the trend expected from absorbing solutions. However, for both microfluidic devices, the reflectance did not change significantly beyond a certain dye concentration. For the 22 μm device, R_{525}/R_{630} finally decays to only 24% of its initial value with almost no change occurring after 50% dye concentration. This effect was much more pronounced in the 44 μm device where the overall decrease in R_{525}/R_{630} is only 11%. This data demonstrates that packaging high concentrations in small volumes decreases the optical path length, thereby causing the light to sample a much lower absorber concentration than it would have in a homogeneous distribution. This is because the optical path length in a homogeneous dye solution is larger than that for the same volume-averaged concentration in the microfluidic device.

For the sake of comparison, we have also indicated the spectral bands (shaded rectangles) that correspond to the absorption coefficient of blood in the Soret (410–430 nm) and *Q*-bands (540–580 nm), assuming a hemoglobin concentration of 150 mg/ml. The range of absorption values used in our experiments compare well with typical hemoglobin values assumed for whole blood. The data shows that the *Q*-bands correspond to a range of values demonstrating minimal flattening, whereas the Soret band experiences a larger degree of flattening. This is also illustrated well in Figure 5 where we present in vivo data from skin. Thus, these plots demonstrate the difficulty of

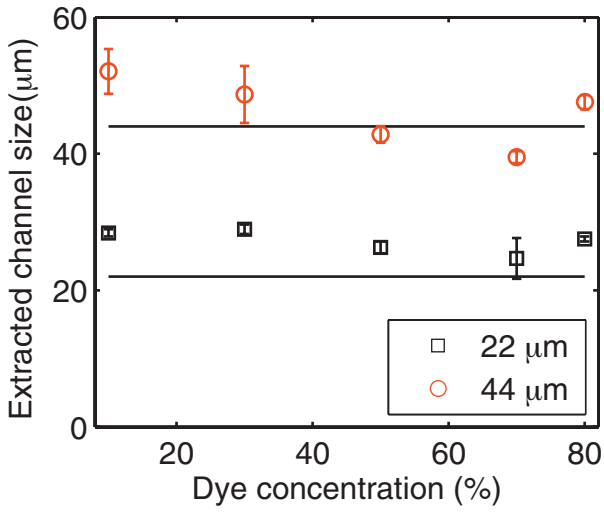

Fig. 5. Measured channel sizes (μm) for both microfluidic devices across all concentrations. Error bars represent 1 SD. The solid lines indicate perfect agreement.

using a homogenous absorption profile to fit data from an inhomogeneous or confined distribution of absorbers.

Although the LUT model measures both scattering and absorption parameters, we will discuss only the absorption properties here. We constrained the absorption coefficient according to Equation (6) and measured the dye concentration. Based on the known dye concentration injected into the channels and the measured value from the inverse model, we calculated a correction ratio (C_{ratio})

$$C_{\text{ratio}} = \frac{\mu_{a(\text{extracted})}}{\mu_{a(\text{expected})}}$$

where μ_a is calculated at 525 nm. We calculated the value of C_{ratio} for each dye concentration for both microfluidic devices. Figure 4d plots the values of C_{ratio} as a function of the optical depth parameter ($2\mu_a r_{\text{vess}}$) discussed earlier. Each point represents an increasing dye concentration in the order described earlier (10%, 30%, 50%, 70%, and 80%). The lower the value of C_{ratio}, the greater the correction required. For both devices, the data demonstrates that the effect of packaging becomes more pronounced as the dye concentration increases. For example, the value of C_{ratio} decreases from 0.8 to 0.23 as dye concentration increases from 10% to 80% for the 22 μm device. In addition, DRS spectra from dye concentrations injected through a 44 μm device required a greater correction than that required for a 22 μm device. For a 10% dye concentration, the C_{ratio} decreased from 0.8 to 0.45 as channel size increased from 22 to 44 μm. Finally, the packaging correction factor, C_{pack}, presented in the Theory Section is plotted once again in Figure 4d to compare it to C_{ratio}. Both C_{pack} and C_{ratio} show good agreement in their dependence on the optical depth parameter ($2\mu_a r_{\text{vess}}$).

We used the LUT-based model and packaging equation to estimate the channel sizes present in the microfluidic device. Figure 5 shows the measured mean vessel diameters across different concentrations. The data shows reasonable agreement between the LUT model and the data for both devices. The average values of the measured channel size for both devices across all phantoms were 27.2 ± 2 and 46.1 ± 5.1 μm, respectively.

In Vivo DRS on Skin

Figure 6a shows a sample diffuse reflectance spectrum from a BCC lesion and adjacent normal skin. There is a large flattening of the trough in the diffuse reflectance spectrum at approximately 420 nm corresponding to the Soret band of hemoglobin absorption. Figure 6b demonstrates two types of fit to the data: (1) no packaging using Equation (1) and (2) packaging corrected using Equation (4). The fit with no packaging underestimates the reflectance in the Soret band. However, on incorporating the correction factor (C_{pack}), the fit improved significantly. We used a residual value to quantify the quality of the fit and incorporating C_{pack} improved the fit by a factor of approximately 10^3. Based on the fits, we determined the

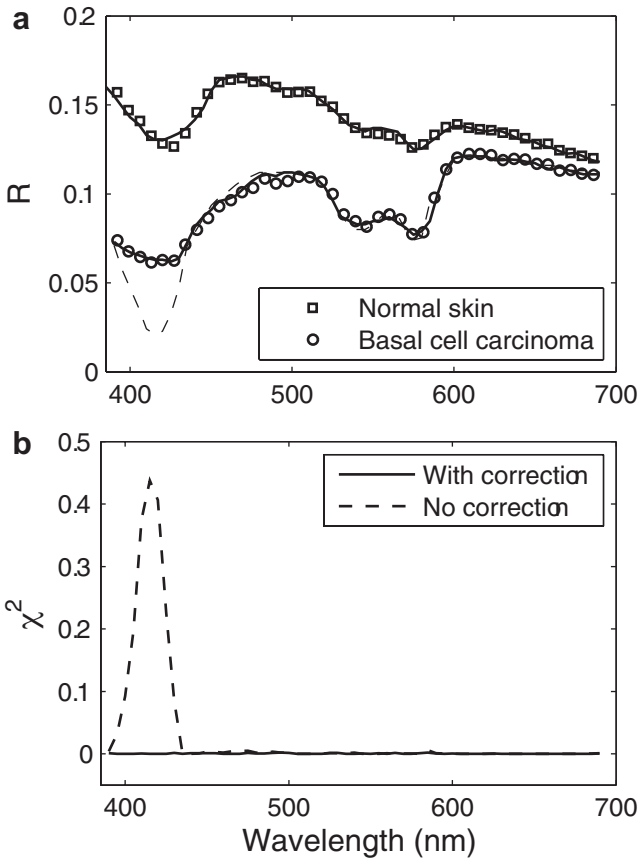

Fig. 6. **a**: Sample diffuse reflectance spectra from normal skin (□) and a BCC lesion (○) and corresponding LUT model fit, with (solid line) and without (dashed line) incorporating packaging in the inverse model. **b**: The fit residuals as a

values of mean vessel diameter for both normal skin and BCC. We use one-way analysis of variance (ANOVA) to determine the statistical significance at $P = 0.05$ level. Our data revealed statistically significant differences in mean vessel diameter and blood volume fraction between normal skin (n = 23) and BCC (n = 39). Figure 7 shows the mean physiological parameters measured from the two groups. Our in vivo studies demonstrate that the change in mean vessel diameter from normal skin ($15 \pm 2\,\mu m$) to BCC ($40 \pm 6\,\mu m$) is statistically significant. Similarly, we also noticed a statistically significant change in the blood volume fraction. These results are consistent with previous reports that demonstrate an increase in blood absorption with progression to cancer [13,19].

DISCUSSION

This paper presents an experimental validation of the effect of pigment packaging on diffuse reflectance measurements over a physiological range relevant to epithelial microvasculature. Studies to date have focused on either Monte–Carlo simulations or experimental measurements using blood vessel-like structures outside the physiological range of vessel sizes found in epithelial microvasculature. We used multi-layer microfluidic devices to simulate a bed of blood vessels with vascular diameters similar to that found in the epithelium.

When discussing the effect of packaging, we tend to focus our attention on the fact that blood is confined to very small structures such as blood vessels. However, it is important to note that the hemoglobin is in fact confined to even smaller structures—red blood cells, which travel inside the blood vessels. Although it is true that the size of the red blood cells is much smaller compared to blood vessels, studies by Finlay and Foster [7] have shown a flattening of the DRS spectra measured from a solution of RBCs. We attempted to study this combined effect by injecting sheep red blood cells (Sigma–Aldrich) through the microfluidic channels. However, due to the design of the openings to the channels and the tendency of the RBCs to aggregate, we were unable to carry out this combined experiment using our model. We anticipate that the smallest diameters of blood vessels in vivo approach the diameter of RBCs. Therefore, we set the lower limit for mean vessel diameter in the LUT-based inverse model to the RBC diameter (5 μm).

The interpretation of mean vessel diameter measured from in vivo spectra deserves some discussion. Tissue microvasculature exists in a complicated capillary bed with a distribution of sizes. The packaging effect in this scenario likely represents some sort of average over the sampled volume. In addition, the measured mean vessel diameter assumes a hemoglobin concentration of 150 mg/ml within the blood and is strongly dependent on this value. For example, if we assume a higher value for hemoglobin concentration in whole blood, the model will estimate lower values for the measured mean vessel diameter and blood volume fraction and vice-versa. Therefore, care must be taken when interpreting the blood volume fraction and mean vessel diameter when the packaging model is used in an inverse fashion to measure these parameters. Both parameters are likely good indicators of the level of packaging and allow us to account for spectral flattening of the diffuse reflectance. Indeed, these models adequately accounted for the distortions in hemoglobin absorption spectra collected from normal and cancerous skin samples. While these pigment packaging models allow for improved fits, we have not ruled out that additional factors may exist that could result in a similar distortion or flattening of the diffuse reflectance spectra. For example, the presence of a highly scattering epidermis (devoid of any blood) can also affect the reflectance spectra in a manner similar to the

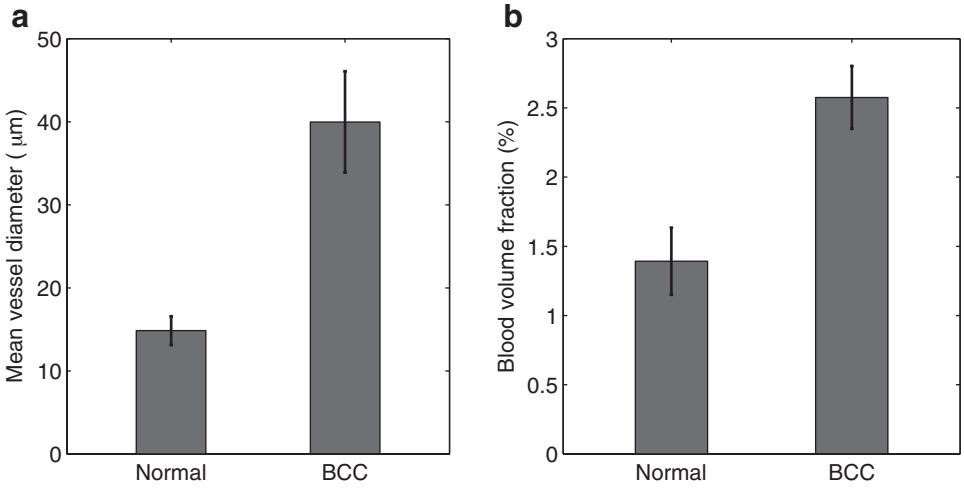

Fig. 7. Measured physiological parameters using the LUT-based inverse model incorporating the packaging correction factor. **a**: Mean vessel diameter (μm) and (**b**) blood volume fraction

presence of blood vessels. A partial volume effect, whereby shorter wavelengths sample shallower depths than longer wavelengths may cause the reflectance to flatten in the Soret band [20]. The shorter wavelengths may sample a lower hemoglobin concentration than the longer wavelengths. Because of the presence of such additional factors that could potentially distort the reflectance spectrum, we are inclined to refer to the term "mean vessel diameter" as hemoglobin packaging factor (HbF) in future studies. We anticipate that future work studying the effects of thin tissue layers mimicking the epithelium using Monte–Carlo simulations and microfluidic phantoms may elucidate the effects of layered geometries on diffuse reflectance spectra as well.

CONCLUSION

We have demonstrated experimental evidence of the pigment packaging effect for tissue epithelial microvasculature. Using microfluidic devices that simulate vessel sizes in a physiological range relevant for epithelial microvessels, we demonstrated significant distortions in the measured reflectance spectra. Our results are consistent with correction factors proposed previously using geometric modeling or analytical equations. In vivo reflectance measurements show that the measured mean vessel diameter and blood volume fraction are significantly higher for NMSC compared to normal skin and could potentially be used as diagnostic parameters for classifying normal skin and NMSC.

ACKNOWLEDGMENTS

Funding for this project was provided by an ASLMS Student Research Grant, an Early Career Translational Research Award from the Wallace H. Coulter Foundation, and a grant from the National Institutes of Health (R01 CA132032). The microfluidic devices fabrication and packaging were carried out at the Microelectronics Research Center (MRC), the University of Texas at Austin.

REFERENCES

1. Farrell TJ, Patterson MS, Wilson B. A diffusion theory model of spatially resolved, steady-state diffuse reflectance for the noninvasive determination of tissue optical properties *in vivo*. Med Phys 1992;19(4):879–888.
2. Tunnell JW, Desjardins AE, Galindo L, Georgakoudi I, McGee SA, Mirkovic J, Mueller MG, Nazemi J, Nguyen FT, Wax A, Zhang Q, Dasari RR, Feld MS. Instrumentation for multi-modal spectroscopic diagnosis of epithelial dysplasia. Technol Cancer Res Treat 2003;2(6):505–514.
3. Palmer GM, Ramanujam N. Monte Carlo-based inverse model for calculating tissue optical properties. Part I: Theory and validation on synthetic phantoms. Appl Opt 2006;45(5): 1062–1071.
4. Reif R, A'Amar O, Bigio I. Analytical model of light reflectance for extraction of the optical properties in small volumes of turbid media. Appl Opt 2007;46(29):7317–7328.
5. Rajaram N, Nguyen TH, Tunnell JW. Lookup table-based inverse model for determining optical properties of turbid media. J Biomed Opt 2008;13(5):050501.
6. Duysens L. The flattening of the absorption spectrum of suspensions, as compared to that of solutions. Biochim Biophys Acta 1956;19(1):1–12.
7. Finlay JC, Foster TH. Effect of pigment packaging on diffuse reflectance spectroscopy of samples containing red blood cells. Opt Lett 2004;29(9):965–967.
8. Svaasand L, Fiskerstrand E, Kopstad G, Norvang L, Svaasand E, Nelson J, Berns M. Therapeutic response during pulsed laser treatment of port-wine stains: Dependence on vessel diameter and depth in dermis. Lasers Med Sci 1995; 10(4):235–243.
9. Verkruysse W, Lucassen G, de Boer J, Smithies D, Nelson J, van Gemert M. Modelling light distributions of homogeneous versus discrete absorbers in light irradiated turbid media. Phys Med Biol 1997;42:51–65.
10. Liu H, Chance B, Hielscher A, Jacques S, Tittel F. Influence of blood vessels on the measurement of hemoglobin oxygenation as determined by time-resolved reflectance spectroscopy. Med Phys 1995;22:1209.
11. van Veen RL, Verkruysse W, Sterenborg HJ. Diffuse–reflectance spectroscopy from 500 to 1060 nm by correction for inhomogeneously distributed absorbers. Opt Lett 2002; 27(4):246–2248.
12. Rajaram N, Aramil TJ, Lee K, Reichenberg JS, Nguyen TH, Tunnell JW. Design and validation of a clinical instrument for spectral diagnosis of cutaneous malignancy. Appl Opt 2010;49(2):142–152.
13. Amelink A, Sterenborg HJ, Bard MP, Burgers SA. *In vivo* measurement of the local optical properties of tissue by use of differential path-length spectroscopy. Opt Lett 2004;29(10): 1087–1089.
14. Reif R, Amorosino M, Calabro K, A'Amar O, Singh S, Bigio I. Analysis of changes in reflectance measurements on biological tissues subjected to different probe pressures. J Biomed Opt 2008;13:010502.
15. Lau C, Scepanovic O, Mirkovic J, McGee S, Yu C, Fulghum S, Jr., Wallace M, Tunnell J, Bechtel K, Feld M. Re-evaluation of model-based light-scattering spectroscopy for tissue spectroscopy. J Biomed Opt 2009;14:024031.
16. Prahl S. Optical absorption of hemoglobin, 1998; http://omlc.ogi.edu/spectra/hemoglobin/index.html.
17. McDonald J, Duffy D, Anderson J, Chiu D, Wu H, Schueller O, Whitesides G. Fabrication of microfluidic systems in poly (dimethylsiloxane). Electrophoresis 2000;21(1): 27–40.
18. Mourant JR, Fuselier T, Boyer J, Johnson TM, Bigio IJ. Predictions and measurements of scattering and absorption over broad wavelength ranges in tissue phantoms. Appl Opt 1997;36(4):949–957.
19. Garcia-Uribe A, Kehtarnavaz N, Marquez G, Prieto V, Duvic M, Wang LV. Skin cancer detection by spectroscopic oblique-incidence reflectometry: Classification and physiological origins. Appl Opt 2004;43(13):2643–2650.
20. Jacques S. Optical assessment of cutaneous blood volume depends on the vessel size distribution: A computer simulation study. J Biophotonics 2009;3(1–2):75–81.